

Small-scale magnetic fields of the spectroscopic binary T Tauri stars V1878 Ori and V4046 Sgr

A. Hahlin and O. Kochukhov

Department of Physics and Astronomy, Uppsala University, Box 516, SE-751 20 Uppsala, Sweden
e-mail: axel.hahlin@physics.uu.se

Received: 13-10-2021, Accepted: 05-01-2022

ABSTRACT

Aims. The goal of this study is to investigate the small-scale magnetic fields of the two spectroscopic binary T Tauri stars V1878 Ori and V4046 Sgr. This is done to complete the observational characterisation of the surface magnetic fields of these stars because only their large-scale magnetic fields have been studied with Zeeman Doppler imaging (ZDI) so far.

Methods. To investigate the small-scale magnetic fields, the differential Zeeman intensification of near-infrared $Ti\ I$ lines was investigated using high-resolution archival spectra obtained with the ESPaDOnS spectrograph at the CFHT. In order to study the binary components separately, the spectra were disentangled by considering observations taken at different orbital phases. The Zeeman-intensification analysis was performed based on detailed polarised radiative transfer calculations aided by the Markov chain Monte Carlo inference, treating magnetic field filling factors and other stellar parameters that could affect the spectra as free parameters.

Results. The obtained average magnetic field strengths of the components of V1878 Ori are 1.33 ± 0.08 and 1.57 ± 0.09 kG, respectively. Previous ZDI studies of V1878 Ori recovered about 14 and 20% of this total magnetic field strength. For V4046 Sgr, the magnetic field strengths are 1.96 ± 0.18 and 1.83 ± 0.18 kG, respectively. In this case, about 12 and 9% of the total magnetic field strength was detected by ZDI.

Conclusions. The small-scale magnetic field strengths obtained from Zeeman intensification are similar for the two components of each binary. This is in contrast to the large-scale magnetic fields obtained from ZDI investigations, performed using the same observations, which found that magnetic field strengths and topologies vary significantly in the components of the two binaries. While the large-scale field might look significantly different, the overall magnetic energy, primarily carried by the small-scale magnetic fields, appears to be quite similar. This indicates that the efficiency of the magnetic dynamo is comparable for the components of the two binaries.

Key words. binaries: spectroscopic – stars: activity – stars: magnetic field – stars: variables: T Tauri – techniques: spectroscopic

1. Introduction

Magnetic fields are important during the early stages of star formation. During the pre-main-sequence, accretion of matter from the surrounding disk onto the star occurs along magnetic field lines (Hartmann et al. 2016). This accretion is accompanied by a corresponding outflow that is required to explain the angular momentum loss that is associated with young stars. This mass outflow was predicted by Matt & Pudritz (2005) to correspond to around 0.1 of the mass accretion for sufficient angular momentum to be lost to explain the rotation rates of young stars. Observations made by Watson et al. (2016) confirmed this theory, finding average outflow accretion ratios close to expected values. The magnetic fields play a role in driving the stellar wind through Alfvén waves (van der Holst et al. 2014). Magnetic fields are also connected to several forms of activity phenomena, such as stellar X-ray emission (Pevtsov et al. 2003). These properties will affect the surrounding environment, such as exoplanets or disks. To understand these aspects of stars, detailed properties of their magnetic fields are needed.

A common method for studying the magnetic fields of stars is Zeeman Doppler imaging (ZDI, Donati & Landstreet 2009; Kochukhov 2016). This method allows reconstructing a vector magnetic field structure on the surface of a rotating star from spectropolarimetric time-series observations. While the information obtained from these studies provides valuable informa-

tion about the global magnetic properties, ZDI does not probe the smaller spatial scales on the stellar surface because the spatial resolution is limited. This limitation is caused by magnetic flux cancellation of nearby surface elements with opposite magnetic polarity, which significantly reduces the observed disk-integrated polarisation signal. For this reason, ZDI is incapable of studying magnetic structures below this limit. A complementary approach to measuring the magnetic field is to use the Zeeman broadening (see e.g. Reiners 2012) by observing changes in the profiles of magnetically sensitive spectral lines. This method does not suffer from the small-scale magnetic signal cancellation that plagues ZDI and provides robust average properties of the magnetic field over the entire surface of late-type stars. Multiple studies comparing results from the two magnetic diagnostic methods have shown that most of the magnetic energy on the surfaces of cool stars is carried within these small-scale magnetic fields (See et al. 2019; Lavail et al. 2019; Kochukhov et al. 2020). For this reason, conclusions about the magnetic field of a star based on the large-scale structure alone are premature.

An application of Zeeman broadening relies on the magnetic field being a dominant contributor to the spectral line broadening. The rapid rotation of active young stars means that magnetic broadening is challenging to detect because the magnetic broadening is smeared out by rotational Doppler broadening. In addition, magnetic broadening is also strongly wavelength de-

pendent, making near-infrared observations preferable. Another property of the magnetic fields can be used in this case, specifically, that magnetic fields will increase the equivalent width of magnetically sensitive lines. This is caused by the desaturation of the lines that occurs due to the Zeeman splitting, effectively allowing more of the stellar flux to be absorbed by the line. This effect is known as Zeeman intensification (e.g. Kochukhov & Lavail 2017; Kochukhov & Shulyak 2019). This approach can be used to obtain information about the magnetic field even for very rapidly rotating stars and using observations at lower wavelengths than typically required for a Zeeman-broadening analysis (see e.g. Hahlin et al. 2021).

In this magnetic field study, two interesting spectroscopic binaries were selected for investigation with the Zeeman-intensification technique, V1878 Ori (Parenago 523, RX J0530.7-0434, 1RXS J053043.1-0434553) and V4046 Sgr (HDE 319139). These binaries are particularly useful because their component masses are similar. The components of V1878 Ori have essentially the same projected mass ($M \sin^3 i$) of $1.54 M_{\odot}$ (Covino et al. 2001; Lavail et al. 2020). Similarly, V4046 Sgr has component masses of 0.91 and $0.87 M_{\odot}$ (Stempels & Gahm 2004). The close similarity between the components in the two binaries and the fact that binary components form simultaneously (Raghavan et al. 2010) means that the conditions within the components should be similar. The magnetic dynamo is thought to be dependent on only a few basic stellar parameters, such as mass and age (Brun & Browning 2017), therefore the magnetic field generation should be similar in the two components of these systems. However, previous ZDI results contradicted this prediction, which might indicate that dynamo processes are different even in almost identical stars. However, as most magnetic energy in late-type stars is carried in small-scale magnetic fields, ZDI might not be the most appropriate method to assess the efficiency of the magnetic dynamo. For this reason, results from a Zeeman-broadening or -intensification analysis could provide additional observational constraints for a comparison of the magnetic field generation in stars with otherwise similar properties.

V1878 Ori is a binary with an eccentric orbit. The two components are intermediate-mass T Tauri stars (IMTTS). IMTTS are progenitors of Herbig Ae/Be stars and eventually A/B-type main-sequence stars. Few of these stars are considered magnetically active; only a few Herbig Ae/Be have detectable magnetic fields (Alecian et al. 2013). In their investigation of the incidence of magnetism among IMTTS, Villebrun et al. (2019) identified a transition region in which the magnetic detection probability shifts from close to 100 % to about 10 %. This occurs when the convective zone is reduced to a mass lower than $\sim 2\%$ of the total mass of the star. The magnetic fields of V1878 Ori have previously been investigated by Lavail et al. (2020). The authors reconstructed the global surface magnetic field maps of the two components. They also performed X-ray observations to determine whether any variation in X-ray activity between periastron and apastron could be observed. The aim was to investigate the extent of magnetospheric interaction during periastron because Getman et al. (2016) found tentative evidence of an increased X-ray activity near periastron. An increased activity could not be confirmed by Lavail et al. (2020), indicating little interaction between the two magnetospheres. The ZDI maps obtained by Lavail et al. (2020) showed significantly different field strengths and topologies of the large-scale fields of the two components. In particular, the average magnetic field strength of the secondary was found to be almost twice as strong as that of the primary component.

V4046 Sgr contains two T Tauri stars with masses very similar to that of the Sun. Therefore, these stars are progenitors to a pair of Sun-like stars. The magnetic fields of the components of V4046 Sgr have also previously been investigated with ZDI by Donati et al. (2011). Similarly to the results for V1878 Ori, the magnetic field maps of V4046 Sgr show a large difference in the field strengths and topologies for the two components. The ZDI maps of both stars have been extrapolated out into the magnetosphere by Gregory et al. (2014), showing connected field lines between the two components. Stempels & Gahm (2004) found periodic variability of emission lines. This was interpreted as a co-rotating gas. Similar flux variability was discovered by Argiroffi et al. (2012) as they studied the system with X-ray observations. This finding supported the magnetically driven accretion scenario as the gas from the circumstellar disk falls down onto the stars along the magnetic field lines.

Because these two systems have already been investigated with ZDI, V1878 Ori by Lavail et al. (2020) and V4046 Sgr by Donati et al. (2011), the large-scale magnetic properties are already well known. In order to complete the picture of the magnetic field, an investigation of the small-scale magnetic field properties is needed.

In Sect. 2 the spectroscopic observations we used in our study of the two binary system are discussed. Section 3 presents the procedure of obtaining disentangled, time-averaged spectra of the individual components. Section 4 discusses the method of extracting information about the magnetic field and determines other relevant stellar parameters. The results of the Zeeman-intensification study of the two components in each binary are also presented in this section. Finally, the overall results of our study are discussed in Sect. 5.

2. Observations

Observations of both stars were obtained at the Canada-France-Hawaii Telescope (CFHT) using the high-resolution spectrograph ESPaDOnS (Donati 2003; Wade et al. 2016). This instrument has a resolving power of 65 000 and covers the wavelength range from 3700 to 10000 Å.

The observations of V1878 Ori were obtained during two periods in 2016, the first between January 14 and 29, and the second between March 25 and 29. These data were collected in the context of the Binarity and Magnetic Interactions in various classes of Stars (BinaMIcS, Alecian et al. 2015) large programme. In total, 25 observations of V1878 Ori are available. A total of 7 observations of V4046 Sgr were obtained in 2009 between September 3 and 9.

The observations of the two binaries are the same as were employed in the ZDI analyses of the global magnetic field topologies of these systems by Lavail et al. (2020) for V1878 Ori and Donati et al. (2011) for V4046 Sgr. That we use the same observations will allow a direct comparison between the small- and large-scale magnetic fields at the same point in time for both systems.

The ESPaDOnS spectra of the two targets were reduced using the UPENA pipeline running the LIBRE-SPIRIT software (Donati et al. 1997). The pipeline data products were downloaded from the CFHT Science Archive hosted by the Canadian Astronomy Data Centre¹. The median signal-to-noise ratio (S/N) of the reduced spectra was estimated for the spectral order centred at 9840 Å, closest to the spectral lines of interest for the

¹ <https://www.cadc-ccda.hia-ihp.nrc-cnrc.gc.ca/en/cfht/>

Table 1. Orbital solutions used for V1878 Ori and V4046 Sgr.

	V1878 Ori ^a	V4046 Sgr ^b
P_{orb} (d)	40.58318 ± 0.00025	2.4213459
T_0 (HJD)	2451098.925 ± 0.065	2446998.335
γ (km s ⁻¹)	32.919 ± 0.066	-6.94
K_A (km s ⁻¹)	47.08 ± 0.18	54.16
K_B (km s ⁻¹)	47.74 ± 0.13	56.61
e	0.3157 ± 0.0018	0.00
ω (deg)	287.45 ± 0.51	0.00

Notes. (a) Lavail et al. (2020), (b) Stempels & Gahm (2004)

Zeeman-intensification analysis. The observations of V1878 Ori have a median S/N of 175, while V4046 Sgr data have a median S/N of 72. A complete list of observations and their S/N can be found in Appendix 5 (Tables A.1 and A.2).

3. Spectral disentangling

Because double-line spectroscopic binaries show a complicated and time-dependent line blending, the spectra of their components need to be disentangled, or separated, to study the components individually. An additional element that needs to be accounted for when interpreting observations in the near-infrared wavelength region is the strong telluric absorption. Here we applied the spectral separation procedure similar to the disentangling performed for other binary systems that have previously been investigated using Zeeman intensification (Kochukhov & Shulyak 2019; Hahlin et al. 2021). Because an orbital solution has already been calculated for the two binary systems (Lavail et al. 2020; Stempels & Gahm 2004, see Table 1), the predicted radial velocity values were used to initiate the disentangling process. The spectral separation procedure was carried out by fitting all available observations simultaneously with a superposition of three spectral components. The first two spectral contributions correspond to the binary components of the system, and the third component represents the telluric absorption. The stellar spectra were shifted according to individual radial velocities and were assumed to be constant. The telluric spectrum was shifted according to the known radial velocity difference of the observatory relative to the heliocentric reference frame and was allowed to vary in intensity to better match individual observations. This composite spectral model was iterated until convergence was achieved, yielding disentangled spectra for both the stellar components and the telluric absorption.

The wavelength region between 9635 and 9816 Å was used for the disentangling process. This wavelength range contains a set of Ti I lines that is useful for Zeeman intensification. These lines are described in more detail in Sect. 4.

The result of this disentangling procedure is a spectrum for each star that corresponds to a mean spectrum averaged over all observations. Examples of these mean spectra are shown in Fig. 1 and 2 for V1878 Ori and V4046 Sgr, respectively. While it would be interesting to obtain phase-resolved intensity spectra to potentially observe variations in magnetic field strength over the rotational period, the time-dependent variability and radial velocity variation of the two components in a spectroscopic binary prevents us from obtaining spectra at each individual phase.

Although our disentangling method is capable of extracting relative radial velocities for the two stellar components at each orbital phase, the absolute radial velocity scale remains unconstrained because no information about laboratory line positions

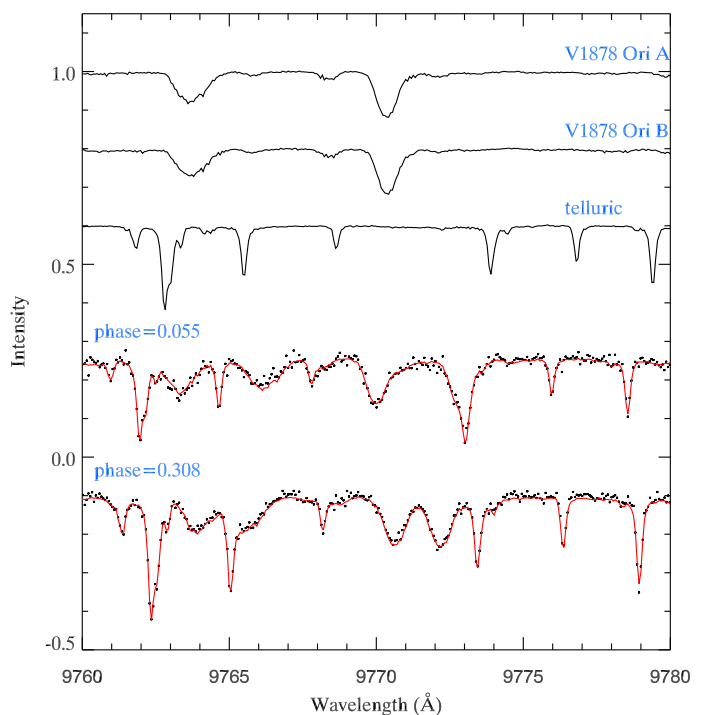


Fig. 1. Illustration of spectral disentangling results for V1878 Ori. The mean spectra of each component are shown at the top, followed by the derived telluric absorption (the third spectrum). The model composite spectra (solid lines) and observations (symbols) at the orbital phases close of the largest and smallest radial velocity separation of the components are compared below. The spectra are shifted vertically for visibility.

is taken into account. If the orbital ephemeris data are inaccurate, the disentangled spectra might be shifted. This appears to be the case for the components of V4046 Sgr in Fig. 2, where the spectral lines that should be at the same wavelength are not aligned. Donati et al. (2011) have encountered similar issues with the orbital ephemeris reported in Stempels & Gahm (2004) in their ZDI study of V4046 Sgr. To mitigate this issue here, we included the radial velocity offset of disentangled spectra as an additional free parameter in the spectrum synthesis modelling.

While the disentangling procedure separates the spectral lines of each component, it is not able to separate the continuum contribution of each star. This causes the absorption lines in the disentangled spectra to be shallower compared to those of a single star. In order to account for this, the luminosity ratio ($LR = L_A/L_B$) of the system must be used to scale either the disentangled or model spectra employed to find the stellar parameters. We opted for scaling the model spectra and derived the luminosity ratio in the investigation of the magnetic field simultaneously with other parameters.

4. Zeeman intensification

The key advantage of Zeeman intensification over Zeeman broadening is that the former magnetic field measurement method concerns itself with only the change in equivalent width of the observed lines and does not attempt to draw information from line profile shapes. This removes the strong preference of observing at longer wavelengths inherent to Zeeman broadening. As a consequence, it becomes easier to use optical spectrographs, which are commonly used for ZDI studies, to perform a simultaneous analysis of the mean magnetic field with the data

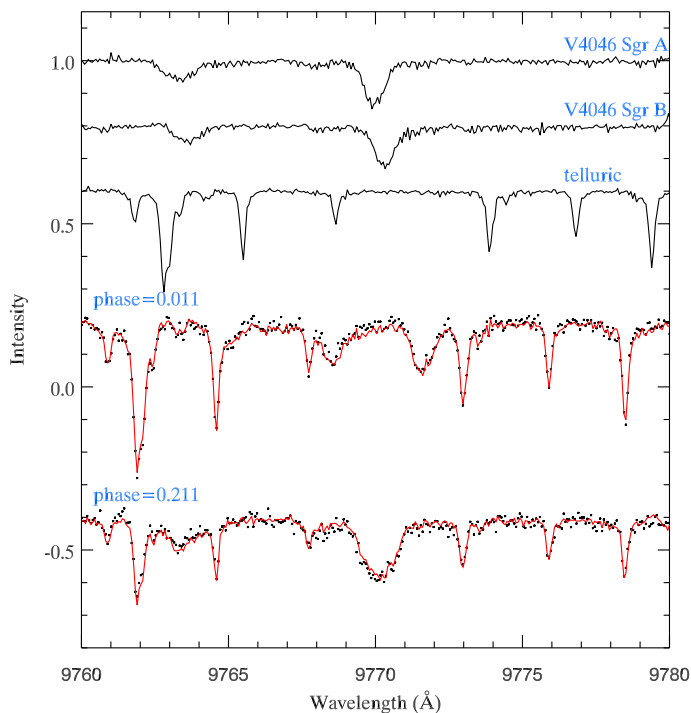


Fig. 2. Same as Fig. 1, but for the spectral disentangling applied to V4046 Sgr.

Table 2. Stellar parameters employed for spectrum synthesis calculations.

	V1878 Ori ^a		V4046 Sgr ^b	
	A	B	A	B
T_{eff} (K)	4800	4750	4370	4100
$\log g$ (cm s^{-2})	4.07	3.84	4.0	4.0
v_{mic} (km s^{-1})	1.0	1.0	1.0	1.0

Notes. (a) Lavail et al. (2020). (b) Stempels & Gahm (2004)

collected for global field mapping. It also removes the requirement that rotational broadening should be low so that it does not hide the magnetic broadening, allowing investigations to be performed even for rapidly rotating active stars using observations with a lower resolution and S/N. A disadvantage with primarily focusing on the equivalent width is that the magnetic effect becomes hard to distinguish from other parameters that modify the line depth, such as the element abundance. This means that magnetically insensitive lines, preferably of the same ion, must be modelled in order to determine non-magnetic parameters simultaneously with the derivation of the magnetic field.

Our study of Zeeman intensification follows previous investigations of the mean magnetic field modulus in G, K, and M stars (Lavail et al. 2019; Kochukhov et al. 2020; Hahlin et al. 2021). The SoBAT library for IDL (Anfinogentov et al. 2021) was used to perform a Markov chain Monte Carlo (MCMC) sampling in order to find a set of parameters that best reproduces observations and establish realistic confidence intervals accounting for possible correlations between parameters. In order to perform this procedure, synthetic spectra were calculated. This was done by collecting line lists from VALD (Ryabchikova et al. 2015), assuming solar metallicity from Asplund et al. (2009), and using MARCS (Gustafsson et al. 2008) model atmospheres in combination with the polarised radiative transfer code Synmast (Kochukhov et al. 2010). Similar to most previous mean

magnetic field studies of cool stars, a uniform radial magnetic field was assumed. This radial assumption will produce a wide range of different magnetic field orientations with respect to the line of sight (Yang & Johns-Krull 2011). As a consequence, any disk-integrated spectrum will contain contributions from several different field directions, giving a balanced contribution to the synthetic spectra. Shulyak et al. (2014) and Kochukhov (2021) showed that replacing a radial field with a horizontal field has little effect on the shape and strength of lines in intensity spectra. For this reason, it is unlikely that our choice of the radial magnetic field geometry has any significant impact on the results presented below.

A grid of synthetic spectra spanning suitable values of Ti abundance and magnetic field strengths was produced for each binary component. The other stellar parameters, T_{eff} , $\log g$, and the microturbulence v_{mic} , were the same as those adopted in previous studies of the two binaries (Stempels & Gahm 2004; Lavail et al. 2020). These parameters are listed in Table 2. The exception are the values of v_{mic} for V1878 Ori. Lavail et al. (2020) obtained significantly different values of v_{mic} for the two components. Because the stars are otherwise similar, this difference is odd. Furthermore, the $v_{\text{mic}} = 2.34 \pm 0.58 \text{ km s}^{-1}$ obtained for the primary star is anomalously high. Typical values of v_{mic} lie in the range of 1.0–1.5 km s^{-1} for cool stars of similar T_{eff} (see e.g. Jofré et al. 2015). A single fixed value of v_{mic} around 1.0 km s^{-1} is frequently assumed in abundance analyses of large samples of late-type stars (e.g. Valenti & Fischer 2005; Brewer et al. 2016). For this reason, we set v_{mic} equal to 1.0 km s^{-1} for the two components of V1878 Ori.

Because the two binaries considered here are T Tauri stars, veiling caused by the accreting matter can significantly affect the stellar spectra by reducing the depth of spectral lines. However, in this particular case, little evidence of strong veiling has been found for either V1878 Ori (Lavail et al. 2020) or V4046 Sgr (Stempels & Gahm 2004). For this reason, we did not include any correction for veiling in our analysis of either binary. In any case, a small veiling correction would be indistinguishable from a change in element abundance.

Ten spectral lines belonging to the same Ti I multiplet formed between the a^5F and z^5F^0 terms of neutral titanium were used in our Zeeman-intensification study. They have been used successfully in past studies of M dwarfs (see Kochukhov & Lavail 2017; Shulyak et al. 2017; Kochukhov & Shulyak 2019). These lines are located in the wavelength interval 9640–9800 Å and have a range of effective Landé factors between 0 and 1.55. The Ti I 9743.61 Å is a magnetic null line, meaning that it is insensitive to a magnetic field. Combining the modelling of this line with the interpretation of magnetically sensitive lines allows disentangling the intensification due to the magnetic field from non-magnetic effects.

Detailed information about the Ti I lines used in our analysis is provided in Table 3. The last column in this table quantifies the relative magnetic sensitivity by comparing the change in equivalent width caused by the introduction of a 1 kG magnetic field. This assessment shows that the Ti I 9688.87 and 9783.59 Å lines in particular have the strongest response to a magnetic field, whereas the Ti I 9743.61 Å line exhibits no response at all, and a handful of lines (9675.54, 9705.67, 9728.41 Å) show a weak response. The 9783.59 Å line, however, is blended with Ti I 9783.31 Å, which reduces the magnetic effect. It is also worthwhile mentioning that while the effective Landé factor is a good indicator of the magnetic sensitivity of spectral lines, it is not always sufficient because Zeeman splitting pattern also plays a

Table 3. Ti I lines used for the Zeeman-intensification analysis.

λ (Å)	E_{lo} (eV)	E_{up} (eV)	$\log gf$	g_{eff}	$\Delta W/W_0^a$
9647.37	0.8181	2.1030	-1.434	1.53	2.64 %
9675.54	0.8360	2.1171	-0.804	1.35	0.85 %
9688.87	0.8129	2.0922	-1.610	1.50	4.98 %
9705.67	0.8259	2.1030	-1.009	1.26	0.99 %
9728.41	0.8181	2.0922	-1.206	1.00	0.84 %
9743.61	0.8129	2.0851	-1.306	0.00	0.00 %
9770.30	0.8484	2.1171	-1.581	1.55	2.85 %
9783.31	0.8360	2.1030	-1.428	1.26	2.22 ^b %
9783.59	0.8181	2.0851	-1.617	1.49	4.97 ^b %
9787.69	0.8259	2.0922	-1.444	1.50	2.53 %

Notes. (a) The relative change in equivalent width caused by a magnetic field strength of 1 kG assuming $T_{\text{eff}} = 4750$, $\log g = 4.0$, $v \sin i = 5 \text{ km s}^{-1}$, and $v_{\text{mic}} = 1 \text{ km s}^{-1}$. (b) Lines are blended; the effective change in equivalent width with both lines combined is 3.34 %.

role. For example, the Ti I 9770.30 Å line has the largest effective Landé factor of the transitions, but not the strongest response to the presence of a magnetic field.

In a change from our previous investigations of Zeeman intensification in the spectra of late-type active binaries (Kochukhov & Shulyak 2019; Hahlin et al. 2021), the inference for the two binary components was performed simultaneously. This is justified by the fact that binaries form together from the same molecular cloud. For this reason, the surface chemical abundances of binary components with a similar mass can be assumed to be the same. By performing the inference simultaneously, these abundances can be constrained by observations of both stars instead of one at a time. In the particular case of V1878 Ori, the metallicities of its components were estimated by Lavail et al. (2020). While a slight difference between the two components was obtained, it was not significant given the uncertainties. This indicates that the Ti abundance of the two stars could be approximated by a single value. The magnetic field is parametrised with a set of N filling factors f_i , representing fractions of the stellar surface covered with a magnetic field of a certain strength B_i ,

$$S_{\text{tot}} = \sum_{i=1}^N f_i S(B_i). \quad (1)$$

Our model is capable of handling any number of magnetic filling factors. For this work, the filling factors are defined in steps of 2 kG, starting at 0 kG. In order to ensure that the magnetic filling factors are properly normalised, they are also constrained according to the equation

$$\sum_{i=1}^N f_i = 1. \quad (2)$$

This prevents the filling factors from covering more or less than the entire star; this solution would not be physical. Because the number of magnetic field filling factors is not known a priori, it is determined by comparing the Bayesian information criterion (BIC, Sharma 2017),

$$\text{BIC} = -2 \ln(Y|\hat{\theta}) + d \ln n, \quad (3)$$

obtained for inferences with different number of filling factors. Here $\ln(Y|\hat{\theta})$ represents the likelihood of the best fit for the spectra Y using the parameters $\hat{\theta}$, d is the number of data points in

the observations for which the inference is performed, and n is the number of parameters used in the inference. This equation weights the accuracy of the fit against the number of parameters used in the inference. The model with the lowest BIC value is selected as the most suitable model for each binary system. This model is found by adding an increasing number of magnetic field components to the model until the BIC value begins to increase, indicating that no further improvement can be made by increasing the complexity of the model.

Because Zeeman intensification is primarily focused on the increase in equivalent width, the magnetic field diagnostic carried out here becomes entangled with other parameters. This means that the inference also includes a determination of the Ti abundance (common for the two binary components) and individual projected rotational velocities $v \sin i$. Because the stars are spectroscopic binaries, the (common) light ratio parameter is also included in order to scale the model spectra to the disentangled spectra according to the following formulas:

$$S_{\text{scaled}}^A = \frac{S_{\text{syn}}^A}{1 + 1/\text{LR}} + \frac{1}{1 + \text{LR}} \quad (4)$$

for the primary, and

$$S_{\text{scaled}}^B = \frac{S_{\text{syn}}^B}{1 + \text{LR}} + \frac{\text{LR}}{1 + \text{LR}} \quad (5)$$

for the secondary. The individual radial velocities are also included to compensate velocity offsets that appear in the disentangling.

In order to ensure that the MCMC walker had sufficient time to find the maximum likelihood region of the parameter space, a burn-in length of 20 000 steps was used. The sampling continued until it reached convergence. This was determined by calculating the effective sample size (ESS; Sharma 2017) from the autocorrelation time of the walker. The requirement for convergence was set to be when the the ESS reached 2000. This convergence was tested every 10 000th step of the walker. The values reported for each star are median values calculated over the obtained posterior distributions. Reported uncertainties correspond to a confidence level of 68%.

4.1. V1878 Ori

The priors for the parameter inference were selected to provide a generous range so as to not interfere with the magnetic field determination. The Ti abundance was given a uniform prior between -6.90 and -7.40 to cover the uncertainties from the two values determined by Lavail et al. (2020). The luminosity ratio in previous studies was assumed to be equal to 1. Here we set a uniform prior of 1 ± 0.5 . With the $v \sin i$ of the two components having similar values, they were both given identical uniform priors corresponding to $15 \pm 2.5 \text{ km s}^{-1}$. All magnetic field filling factors were given uniform priors between 0 and 1, with the additional constraint defined by Eq. (2). As discussed in Sect. 3, the lines in disentangled spectra might be slightly shifted from their expected laboratory positions. Even if there is no obvious shift for either component of V1878 Ori, the radial velocities of the two components were allowed to vary in a range of $\pm 2 \text{ km s}^{-1}$ in order to ensure that the shift did not affect the final result.

The magnetic field was studied using models with a different number of magnetic filling factors. The model chosen was the model with lowest BIC value as calculated from Eq. (3). The obtained BIC values for all models are listed in Table B.1. For V1878 Ori, the optimal number of parameters was a total of

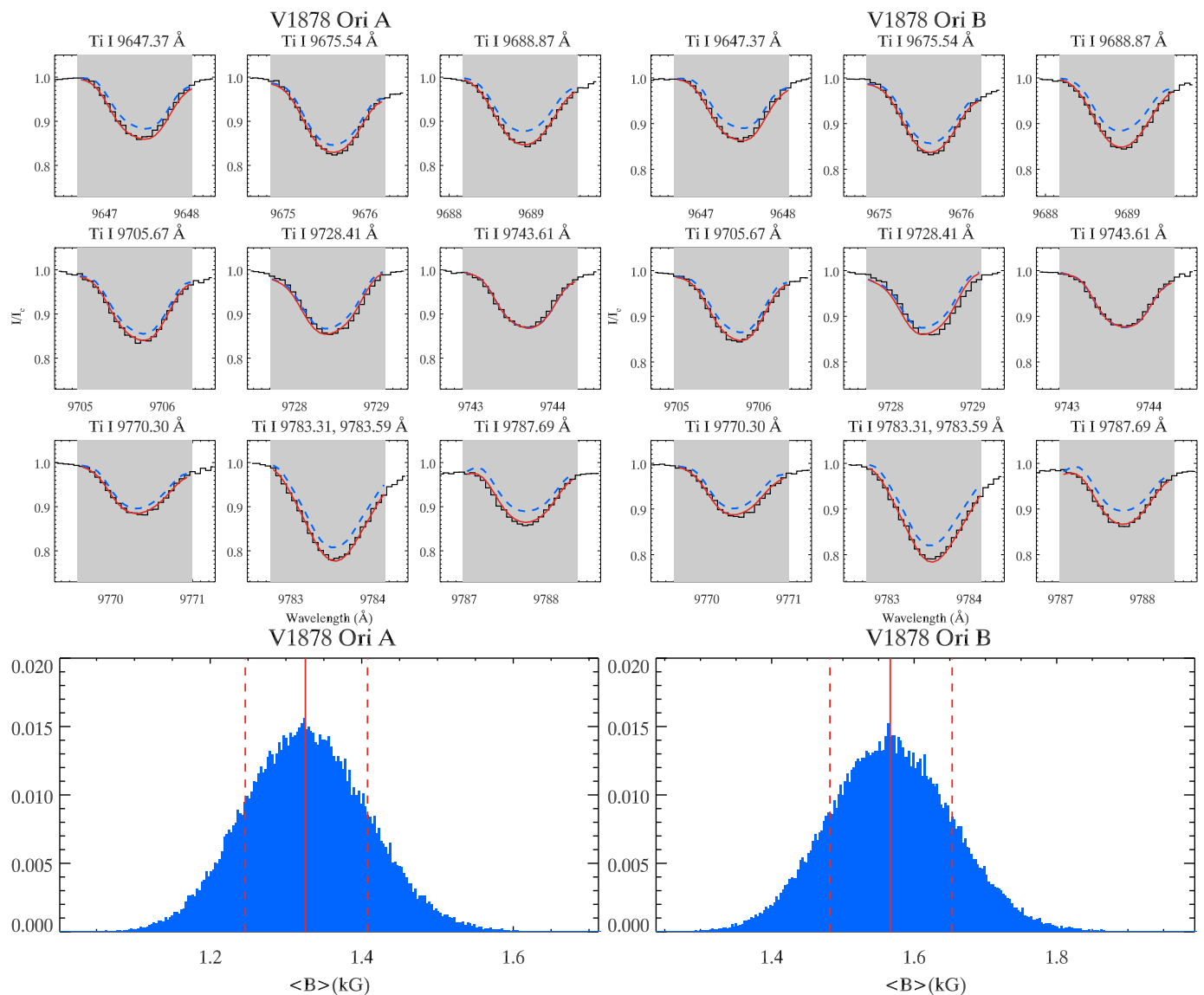


Fig. 3. Inference result for V1878 Ori *Top*. Fit to the observed spectral lines (black histograms) with the spectra corresponding to the best-fitting parameters (solid red line). The dashed blue lines correspond to theoretical spectra without accounting for the magnetic field. Central wavelengths in Å of each line are given above the corresponding panels. *Bottom*. Posterior distribution of the average surface magnetic field strength in the components of V1878 Ori. The vertical lines show the median (solid line) value and 68% percentile (dashed lines).

three filling factors for each component, corresponding to field strengths of 0, 2, and 4 kG, respectively. The resulting parameters from the inference are listed in Table 4. The best fit to spectral lines and the posterior distribution of the average magnetic field is presented in Fig. 3. The complete inference result in the form of posterior distributions of the selected parameters is shown in the appendix, Fig. B.1. Some inference parameters are correlated with each other. The filling factors of different magnetic field strengths are connected because the intensification is primarily sensitive to the average magnetic field strength. The filling factors and $v \sin i$ are also correlated. Because the correlation between $v \sin i$ and f_4 is negative and that between $v \sin i$ and f_2 is negative, it indicates an interplay between magnetic and rotational broadening in these Ti I lines. The mean magnetic field strength of V1878 Ori B is slightly higher than that of V1878 Ori A: 1.57 ± 0.09 versus 1.33 ± 0.08 kG.

The two overall metallicities $[M/H]$ determined by Lavail et al. (2020) were 0.06 ± 0.17 and -0.07 ± 0.26 for V1878 Ori A and B, respectively. Assuming Ti follows this general trend,

these values correspond to Ti abundances of -7.03 and -7.16 in the $\log(N_{\text{Ti}}/N_{\text{tot}})$ units, respectively. Our joint Ti abundance agrees with these two values within the uncertainties. This indicates that the titanium abundances in the two components in the V1878 Ori system can be described by a single value. The other parameters obtained through the inference also agree with the values previously determined by Lavail et al. (2020).

4.2. V4046 Sgr

The priors for V4046 Sgr were selected in a similar way as for V1878 Ori. The primary difference is that Stempels & Gahn (2004) estimated the luminosity ratio of the system to be 1.5. While this value was determined in a different wavelength range than we used in the current study, it does indicate that there is a noticeable difference between the brightness of the two stars. Consequently, the uniform luminosity ratio prior was chosen as 1.5 ± 0.5 . An abundance prior between -6.90 and -7.80 dex was selected. There seems to be a large radial velocity shift in the

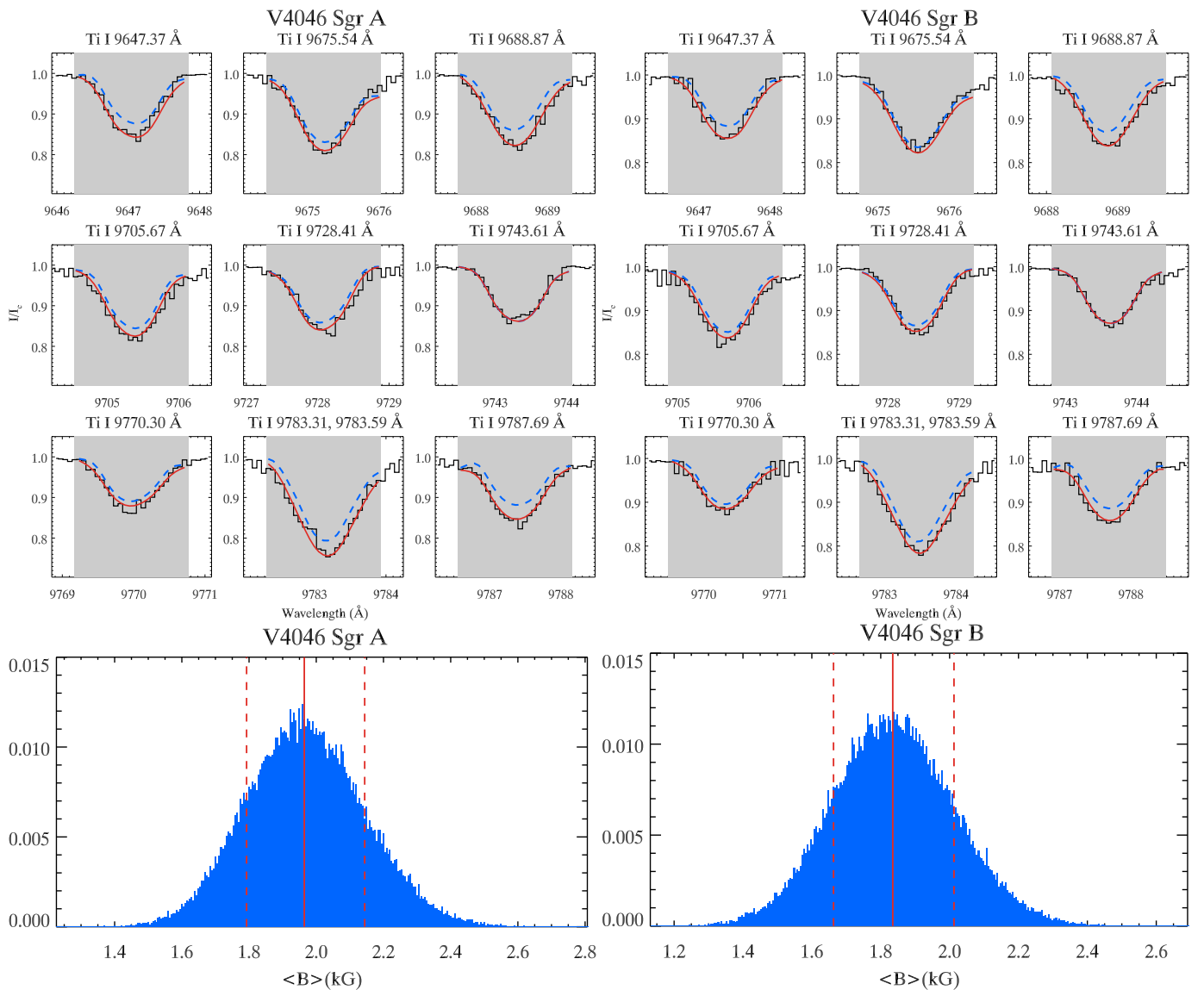


Fig. 4. Results for V4046 Sgr presented in the same way as for V1878 Ori in Fig. 3.

Table 4. Obtained parameters for the components of V1878 Ori.

Parameter	A	B
$\langle B_l \rangle$ (kG)	1.33 ± 0.08	1.57 ± 0.09
f_0	0.50 ± 0.04	0.37 ± 0.04
f_2	0.34 ± 0.07	0.47 ± 0.07
f_4	0.16 ± 0.04	0.16 ± 0.04
$v \sin i$ (km s $^{-1}$)	14.14 ± 0.14	13.32 ± 0.15
ε_{Ti}	-6.93 ± 0.02	
LR	1.08 ± 0.02	

Notes. f_0 is determined from eq. 2

disentangled spectra of V4046 Sgr B. For this reason, its radial velocity was first adjusted by eye and was then allowed to vary in a range of ± 2 km s $^{-1}$. The prior for $v \sin i$ was set as ± 2.5 km s $^{-1}$ around the values used by previous studies (Quast et al. 2000; Stempels & Gahm 2004).

Similarly to V1878 Ori, the most suitable model according to the BIC was a model containing three filling factors, corresponding to 0, 2, and 4 kG, for the magnetic field on each star

(see Table B.1). The parameter values are reported in Table 5, with the best fit to observations and the average magnetic field posterior distributions shown in Fig. 4. Complete posterior distributions are also available in the appendix (Fig. B.2). The correlations between the inference parameters are qualitatively similar to those seen for V1878 Ori. The mean magnetic fields at the surface of the two components are similar in strength: 1.96 ± 0.18 and 1.83 ± 0.18 kG for components A and B, respectively.

The luminosity ratio obtained here is slightly lower than what was determined by Stempels & Gahm (2004). This is likely explained by the fact that the observations analysed here correspond to a wavelength interval farther to the red compared to the analysis by Stempels & Gahm (2004). The $v \sin i$ values that we derived are slightly higher than what has been obtained by previous studies (Stempels & Gahm 2004; Donati et al. 2011). The reason might be that other broadening parameters (such as macroturbulence) are not accounted for in our inference, which can lead to an overestimation of the stellar rotation rate.

Overall, our results for V4046 Sgr have larger uncertainties than for V1878 Ori. This difference comes from two sources. First, the S/Ns of the individual observations for V4046 Sgr are significantly lower than those for V1878 Sgr (see Table A.1 and

Table 5. Obtained parameters for the components of V4046 Sgr.

Parameter	A	B
$\langle B_I \rangle$ (kG)	1.96 ± 0.18	1.83 ± 0.18
f_0	0.42 ± 0.07	0.45 ± 0.08
f_2	0.17 ± 0.12	0.18 ± 0.15
f_4	0.40 ± 0.07	0.37 ± 0.08
$v \sin i$ (km s ⁻¹)	15.1 ± 0.3	14.4 ± 0.3
ε_{Ti}	-7.68 ± 0.03	
LR	1.27 ± 0.04	

Notes. f_0 is determined from Eq. 2.

Table 6. Inference results for V1878 Ori using different values of v_{mic} .

Parameter	A		B		A		B	
	A	B	A	B	A	B	A	B
v_{mic} (km s ⁻¹)	0.5		1.0		1.5			
ε_{Ti}	-6.69		-6.93		-7.16			
$\ln(Y \hat{\theta})$	1507 ± 2.7		1509 ± 2.6		1505 ± 2.6			
$\langle B_I \rangle$ (kG)	1.25	1.40	1.33	1.57	1.67	1.94		

A.2). The second reason is that the observations were then combined into the mean intensity spectra (see Sect. 3). There are in total 25 observations for V1878 Ori, but only eight for V4046 Sgr, which further contributes to the noise difference in the mean disentangled spectra.

4.3. Impact of microturbulent velocity

While our choice of v_{mic} is in line with the results of studies of other stars with similar atmospheric parameters, it would be interesting to assess how different choices would affect our results. To this end, we recalculated synthetic spectra for different values of v_{mic} in the range of 0.5–1.5 km s⁻¹ and repeated the magnetic inference described above. This analysis was only performed for the observations of V1878 Ori. Because the stellar atmospheres used for the two T Tauri systems are similar, the effect of changing v_{mic} should also be similar for the two binary systems. A few key parameters to evaluate the impact of different assumptions about v_{mic} are summarised in Table 6.

Some variation between the outcomes of inferences with different v_{mic} was detected. Because the primary effect of v_{mic} is to increase the line depth, both the abundance and magnetic field strengths were affected. The Ti abundance varied by about 0.2 dex for a change in v_{mic} by 0.5 km s⁻¹. For the same variation of v_{mic} , the magnetic field changed by 0.08–0.37 kG, with a larger change corresponding to the variation of v_{mic} from 1.0 to 1.5 km s⁻¹. The quality of the fit with different v_{mic} values was also assessed using the likelihood (see parameter $\ln(Y|\hat{\theta})$ in Table 6). We found the likelihood to be highest for $v_{\text{mic}} = 1$ km s⁻¹. This difference in likelihood, however, is not significant when the 68% confidence intervals of the inferences with different v_{mic} values are considered. To summarise, the set of Ti I lines does not provide a strong independent constraint on v_{mic} , likely because these lines do not differ much in terms of their intensities.

The uncertainty in the choice of v_{mic} increases the uncertainties of the inference results, particularly for the Ti abundance and the magnetic field strength. The additional uncertainty is larger than what was obtained from the inference (see Table 4), which highlights the importance of accurate model assumptions. Anderson et al. (2010) also investigated the impact on magnetic field determination when changing stellar models. They considered the correlation of different stellar model parameters and av-

erage magnetic strength. In their results, they also found correlations between v_{mic} and $\langle B_I \rangle$, where a shift in a few hundred Gauss corresponded to a few tenths of km s⁻¹, similar to our results.

However, this uncertainty does not have a significant impact on the relative difference between the magnetic field strengths of the two binary components. The relative field strength for V1878 Ori components, $\langle B_I \rangle_A / \langle B_I \rangle_B$, remains in the range of 0.85 to 0.9 for all three assumed v_{mic} values. For this reason, our analysis results should still be highly reliable at least for a comparison of the magnetic properties of the two components.

5. Summary and discussion

This work has presented the magnetic field analysis for two spectroscopic binaries, the T Tauri stars V1878 Ori and V4046 Sgr. By using multiple high-resolution observations, we were able to disentangle the spectra, remove telluric lines, and perform a detailed Zeeman-intensification analysis for each component. This allowed the determination of several stellar parameters as well as the properties of the small-scale magnetic field for the two components in the two binaries. By using the same observations as ZDI studies of these stars, we are now in the position to compare characteristics of the large- and small-scale magnetic fields more directly than was possible in previous studies (e.g. Lavail et al. 2019).

Many previous studies showed that the magnetic field strengths recovered by ZDI are low, typically about 5–20% compared to the field strength determined using Zeeman-intensification or -broadening analysis (See et al. 2019; Kochukhov et al. 2020). For T Tauri stars, the situation is slightly different; ZDI recovers more than 40% of the magnetic field strength for some stars (Lavail et al. 2019). The mean magnetic field strengths for the components of V1878 Ori obtained using ZDI by Lavail et al. (2020) are 180 and 320 G for components A and B, respectively. Compared to our results of 1.33 ± 0.08 and 1.57 ± 0.09 kG, about 14 and 20% of the magnetic flux from Zeeman intensification was recovered with ZDI for the respective components. For V4046 Sgr, the ZDI study by Donati et al. (2011) reported average global magnetic field strengths of 230 and 170 G for components A and B, respectively. Compared to our results of 1.96 ± 0.18 and 1.83 ± 0.18 kG, the ZDI magnetic fields correspond to about 12 and 9% of the total magnetic flux revealed by our Zeeman-intensification analysis. These values are in line with previously established trends, although care should be taken when relations obtained for main-sequence stars are extended to pre-main-sequence objects.

In the Zeeman-broadening study of T Tauri stars, Lavail et al. (2019) found that the field strength recovery capabilities of ZDI improve for simple, axisymmetric field geometries. The two components of V1878 Ori have relatively simple field geometries, and ZDI recovers a larger fraction of the total magnetic field than for the V4046 Sgr components, which have more complicated global field structures. However, Lavail et al. (2020) found that V1878 Ori A has a very weak contribution of axisymmetric magnetic field components (8.5% of the total magnetic energy). This indicates that the simplicity of the magnetic field structure rather than degree of axisymmetry might be a more important factor in determining the ability of ZDI to infer a realistic total field strength. Because the spread between results obtained for similar stars is often quite large, more investigations about the field recovery fraction of ZDI in T Tauri stars could clarify these matters.

The average magnetic field strengths of the two components in the two binary stars are very similar. In addition, the magnetic

filling factors corresponding to different magnetic field strengths are similar for the components (see Table 4 and 5). This further highlights the similarity between the properties of small-scale magnetic fields of the components because a similar filling factor distribution, in combination with a similar average field strength, indicates that the magnetic energies should be similar. On the other hand, the magnetic field strength distribution is different between V1878 Ori and V4046 Sgr. For the first system, the magnetic field is dominated by weaker field components, while the second system has higher contributions of stronger magnetic fields at the surface.

The similarity of the small-scale fields obtained for the binary components in this work can be compared with the significantly different global magnetic field strength and geometries obtained for V1878 Ori (Lavail et al. 2020) and V4046 Sgr (Donati et al. 2011) using ZDI. Lower-mass binary systems, with a mass ratio close to one, where both the global magnetic field geometry and the total field strength were investigated simultaneously (e.g. Kochukhov & Lavail 2017; Kochukhov & Shulyak 2019), also show smaller variations in the total strength obtained from the broadening and intensification of spectral lines than the average strength of the field recovered by ZDI. This pattern appears to be consistently present in binary stars of different sizes and evolutionary stages. Both partially and fully convective stars also seem to follow this trend. With similar initial conditions and mass, it is likely that the magnetic fields of the stars we studied are functionally similar, but that the constant evolution of the large-scale magnetic field geometry during magnetic cycles makes the ZDI result more dependent on when the star is observed rather than what type of star is observed. Repeated spectropolarimetric observations, such as those performed for single stars by Boro Saikia et al. (2018), of binaries containing components with similar stellar parameters could clarify whether this dichotomy is just temporal in nature or a fundamental property of the different binary components. Combining the multi-epoch spectropolarimetric studies with simultaneous Zeeman-broadening or -intensification investigations could further improve the understanding of the magnetic field evolution of stars by determining how the overall magnetic energy changes over different timescales.

In the near future, observations from the new generation of near-infrared spectropolarimeters such as SPIrou (Donati et al. 2020) and CRILES⁺ (Dorn et al. 2016) could give new insight into the magnetic fields of cool stars. With a high resolution and a large spectral grasp, these spectropolarimeters should be capable of providing data for simultaneous investigations of both small- and large-scale magnetic fields. The fact that these spectropolarimeters are operating at near-infrared wavelengths will also make any Zeeman-broadening signatures easier to detect. The result of this work highlights one question in particular that could be investigated by these future studies, that is, the similarity of the magnetic fields of stellar twins. Binary stars provide the best laboratories to answer this question as similar stellar parameters and origin reduce any potential variations that could otherwise impact the magnetic field generation, allowing a direct comparison.

Acknowledgements. We thank the referee for their comments. This study is supported by the Swedish Research Council, the Swedish Royal Academy of Sciences, and the Swedish National Space Board. The observational data analysed in this work were obtained at the Canada-France-Hawaii Telescope (CFHT), which is operated by the National Research Council of Canada, the Institut National des Sciences de l'Univers of the Centre National de la Recherche Scientifique of France, and the University of Hawaii.

References

- Alecian, E., Neiner, C., Wade, G. A., et al. 2015, in IAU Symposium, Vol. 307, *New Windows on Massive Stars*, ed. G. Meynet, C. Georgy, J. Groh, & P. Stee, 330–335
- Alecian, E., Wade, G. A., Catala, C., et al. 2013, *MNRAS*, 429, 1001
- Anderson, R. I., Reiners, A., & Solanki, S. K. 2010, *A&A*, 522, A81
- Anfinogentov, S. A., Nakariakov, V. M., Pascoe, D. J., & Goddard, C. R. 2021, *ApJS*, 252, 11
- Argiroffi, C., Maggio, A., Montmerle, T., et al. 2012, *ApJ*, 752, 100
- Asplund, M., Grevesse, N., Sauval, A. J., & Scott, P. 2009, *ARA&A*, 47, 481
- Boro Saikia, S., Lueftinger, T., Jeffers, S. V., et al. 2018, *A&A*, 620, L11
- Brewer, J. M., Fischer, D. A., Valenti, J. A., & Piskunov, N. 2016, *ApJS*, 225, 32
- Brun, A. S. & Browning, M. K. 2017, *Living Reviews in Solar Physics*, 14, 4
- Covino, E., Melo, C., Alcalá, J. M., et al. 2001, *A&A*, 375, 130
- Donati, J. F. 2003, in *Astronomical Society of the Pacific Conference Series*, Vol. 307, *Solar Polarization*, ed. J. Trujillo-Bueno & J. Sanchez Almeida, 41
- Donati, J. F., Gregory, S. G., Montmerle, T., et al. 2011, *MNRAS*, 417, 1747
- Donati, J. F., Kouach, D., Moutou, C., et al. 2020, *MNRAS*, 498, 5684
- Donati, J. F. & Landstreet, J. D. 2009, *ARA&A*, 47, 333
- Donati, J. F., Semel, M., Carter, B. D., Rees, D. E., & Collier Cameron, A. 1997, *MNRAS*, 291, 6980
- Dorn, R. J., Follert, R., Bristow, P., et al. 2016, in *Society of Photo-Optical Instrumentation Engineers (SPIE) Conference Series*, Vol. 9908, *Ground-based and Airborne Instrumentation for Astronomy VI*, ed. C. J. Evans, L. Simard, & H. Takami, 99080I
- Getman, K. V., Broos, P. S., Kóspál, Á., Salter, D. M., & Garmire, G. P. 2016, *AJ*, 152, 188
- Gregory, S. G., Holzwarth, V. R., Donati, J. F., et al. 2014, in *Magnetic Fields throughout Stellar Evolution*, ed. P. Petit, M. Jardine, & H. C. Spruit, Vol. 302, 44–45
- Gustafsson, B., Edvardsson, B., Eriksson, K., et al. 2008, *A&A*, 486, 951
- Hahlin, A., Kochukhov, O., Alecian, E., Morin, J., & BinaMICS Collaboration. 2021, *A&A*, 650, A197
- Hartmann, L., Herczeg, G., & Calvet, N. 2016, *ARA&A*, 54, 135
- Jofré, P., Heiter, U., Soubiran, C., et al. 2015, *A&A*, 582, A81
- Kochukhov, O. 2016, *Doppler and Zeeman Doppler Imaging of Stars*, ed. J.-P. Rozelot & C. Neiner, Vol. 914, 177
- Kochukhov, O. 2021, *A&A Rev.*, 29, 1
- Kochukhov, O., Hackman, T., Lehtinen, J. J., & Wehrhahn, A. 2020, *A&A*, 635, A142
- Kochukhov, O. & Lavail, A. 2017, *ApJ*, 835, L4
- Kochukhov, O., Makaganiuk, V., & Piskunov, N. 2010, *A&A*, 524, A5
- Kochukhov, O. & Shulyak, D. 2019, *ApJ*, 873, 69
- Lavail, A., Kochukhov, O., & Hussain, G. A. J. 2019, *A&A*, 630, A99
- Lavail, A., Kochukhov, O., Hussain, G. A. J., et al. 2020, *MNRAS*, 497, 632
- Matt, S. & Pudritz, R. E. 2005, *ApJ*, 632, L135
- Pevtsov, A. A., Fisher, G. H., Acton, L. W., et al. 2003, *ApJ*, 598, 1387
- Quast, G. R., Torres, C. A. O., de La Reza, R., da Silva, L., & Mayor, M. 2000, *IAU Symposium*, 200, 28
- Raghavan, D., McAlister, H. A., Henry, T. J., et al. 2010, *ApJS*, 190, 1
- Reiners, A. 2012, *Living Reviews in Solar Physics*, 9, 1
- Ryabchikova, T., Piskunov, N., Kurucz, R. L., et al. 2015, *Phys. Scr*, 90, 054005
- See, V., Matt, S. P., Folsom, C. P., et al. 2019, *ApJ*, 876, 118
- Sharma, S. 2017, *ARA&A*, 55, 213
- Shulyak, D., Reiners, A., Engeln, A., et al. 2017, *Nature Astronomy*, 1, 0184
- Shulyak, D., Reiners, A., Seemann, U., Kochukhov, O., & Piskunov, N. 2014, *A&A*, 563, A35
- Stempels, H. C. & Gahm, G. F. 2004, *A&A*, 421, 1159
- Valenti, J. A. & Fischer, D. A. 2005, *ApJS*, 159, 141
- van der Holst, B., Sokolov, I. V., Meng, X., et al. 2014, *ApJ*, 782, 81
- Villebrun, F., Alecian, E., Hussain, G., et al. 2019, *A&A*, 622, A72
- Wade, G. A., Neiner, C., Alecian, E., et al. 2016, *MNRAS*, 456, 2
- Watson, D. M., Calvet, N. P., Fischer, W. J., et al. 2016, *ApJ*, 828, 52
- Yang, H. & Johns-Krull, C. M. 2011, *ApJ*, 729, 83

Appendix A: List of spectroscopic observations**Table A.1.** ESPaDOnS observations of V1878 Ori.

Reduced HJD	S/N	Reduced HJD	S/N
57401.295	180	57409.301	176
57401.462	153	57410.380	183
57402.224	181	57411.335	191
57402.451	171	57412.361	171
57403.268	188	57413.345	182
57403.449	178	57414.383	184
57404.286	188	57415.384	181
57404.451	173	57416.344	189
57405.262	196	57472.232	153
57405.378	192	57474.232	158
57406.364	192	57475.232	143
57407.287	172	57476.232	132
57408.401	159		

Table A.2. ESPaDOnS observations of V4046 Sgr.

Reduced HJD	S/N
55077.273	66
55078.316	64
55079.221	75
55080.220	78
55080.313	80
55081.221	60
55082.222	78
55083.221	82

Table B.1. BIC values for different field parameterisation models.

N	BIC	
	V1878 Ori	V4046 Sgr
2	-2109.60	-1742.01
3	-2117.19	-1743.16
4	-2070.95	-1700.56

Appendix B: Inference results

Models containing up to four different magnetic field components were compared. This corresponds to a superposition of synthetic spectra computed for magnetic field strengths of 0, 2, 4, and 6 kG. The resulting BIC values calculated using the Eq. (3) are reported in Table B.1. The difference between the first two models are not particularly large, while the model with the most magnetic field components has noticeably higher BIC values. This indicates that including the 4 kG component does improve the fit quality sufficiently to mitigate the complexity of the model, while adding the 6 kG component has a very marginal effect on the fit quality. Figures B.1 and B.2 show the posterior distributions of parameters for the model with the lowest BIC and three magnetic field components that were used to analyse the magnetic fields of the two binary stars.

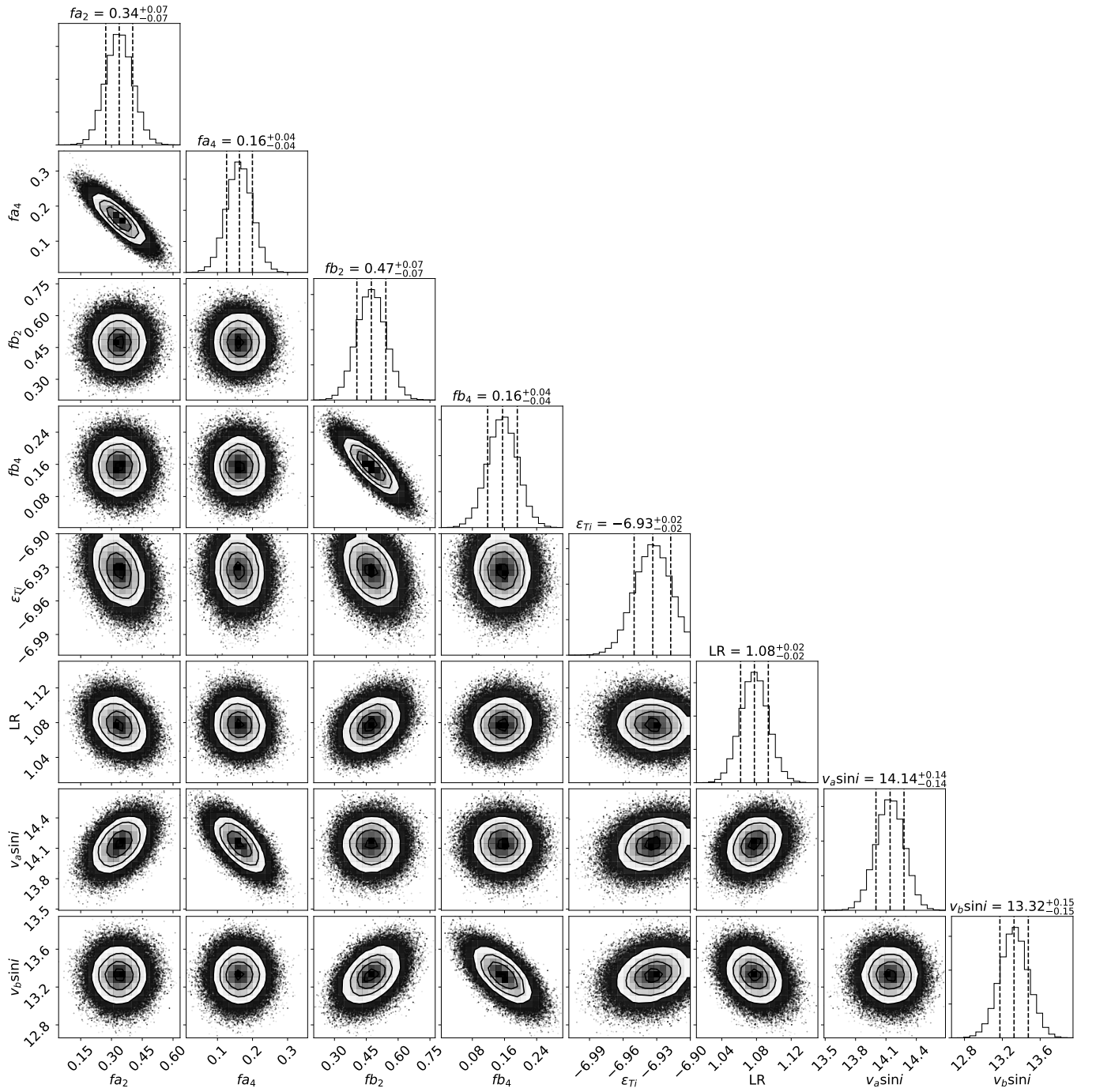


Fig. B.1. Inference result for V1878 Ori showing the posterior distributions for the parameters derived with a simultaneous fit to the observed spectra of the two components.

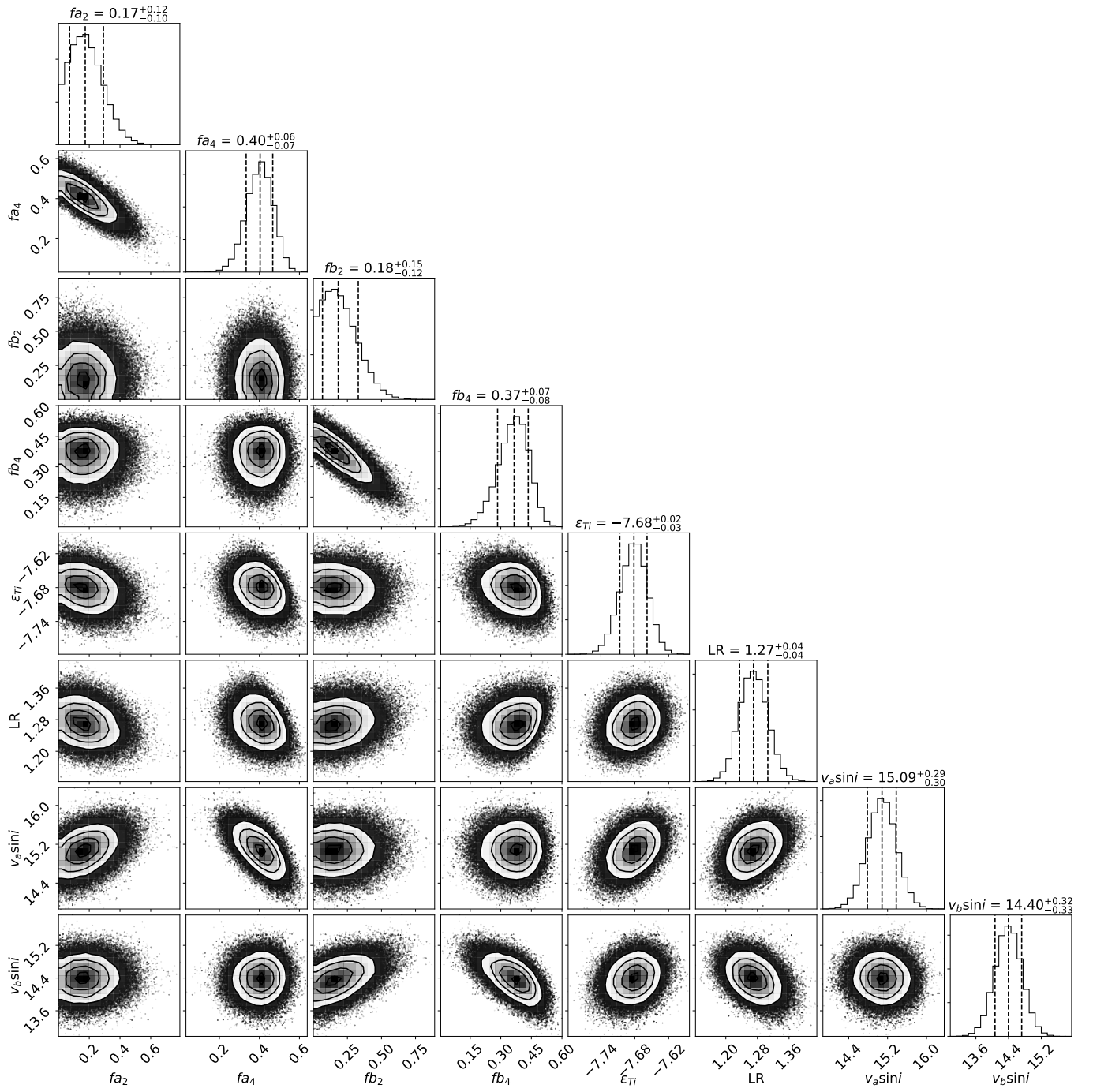


Fig. B.2. Inference result for V4046 Sgr presented in the same way as for V1878 Ori in Fig. B.1.